

Linear comparison of gyrokinetic codes with trapped electrons

G. Rewoldt^{a,*}, Z. Lin^b, Y. Idomura^c

^a Princeton Plasma Physics Laboratory, Princeton, NJ, USA

^b University of California at Irvine, Irvine, CA, USA

^c Japan Atomic Energy Agency, Higashi-Ueno 6-9-3, Taitou, Tokyo 110-0015, Japan

Received 3 November 2006; received in revised form 19 April 2007; accepted 16 June 2007

Available online 17 July 2007

Abstract

Three codes that solve the gyrokinetic equation in toroidal geometry are compared in the linear limit for the growth rates and real frequencies of the ion temperature gradient (ITG) mode and the trapped electron mode (TEM). The three codes are the gyrokinetic toroidal code (GTC) and GT3D, both of which are radially-global particle-in-cell initial-value codes, and FULL, which is a radially-local continuum eigenvalue code. With the same standard input parameters on a reference magnetic surface, the three codes give good agreement for the linear eigenfrequencies, both without (i.e. with adiabatic electron response) and with trapped electrons, as the perpendicular wavenumber and the ion temperature gradient input parameters are varied.

© 2007 Elsevier B.V. All rights reserved.

PACS: 52.65Tt; 52.54Rr; 52.55fa

Keywords: Vlasov–Poisson; Gyrokinetic; Trapped electron mode; Ion temperature gradient mode

1. Introduction

Here we compare results in the linear limit from three distinct codes that solve the gyrokinetic equation, the gyrokinetic toroidal code (GTC) [1], the GT3D code [2], and the FULL code [3,4]. The GTC and GT3D codes are radially-global, linear or nonlinear, particle-in-cell initial-value codes, while the FULL code is a radially-local linear continuum eigenvalue code which employs the ballooning representation [5]. The GTC code as described in Ref. [1] and the GT3D code as described in Ref. [2] had purely adiabatic electron response, $n_e = -(en_0/T_e)(\Phi - \langle\Phi\rangle)$, where Φ is the electrostatic potential and $\langle\dots\rangle$ denotes a flux-surface average. Extensions of GTC and GT3D to include effects of trapped electrons will be described here. The FULL code has always included the complete electron response, which is described in Refs. [3] and [4], including the effects of trapped electrons. The linear eigenfrequency results from the FULL code have previously been compared several times with those from a corresponding radially-

local initial-value code, with good agreement [6–8]. The GTC code uses a local Maxwellian equilibrium distribution function for both linear and nonlinear simulations when using uniform marker particles, while the GT3D code uses a local Maxwellian equilibrium distribution function for linear simulations but uses a canonical Maxwellian equilibrium distribution function for nonlinear simulations [2]. The FULL code also uses a local Maxwellian equilibrium distribution function.

An extension of the GTC code to include trapped electron effects is described in Section 2, as well as a corresponding extension of the GT3D code. The case used for this comparison is described in Section 3. Results in the adiabatic electron limit and results with trapped electrons are presented in Section 4. Conclusions are given in Section 5.

2. Trapped-electron extensions for GTC and GT3D codes

GTC is a full torus, particle-in-cell code for simulating low frequency turbulence in fusion plasmas. The guiding center equations of motion are derived from a Hamiltonian formulation [9]. The gyrokinetic Poisson Equation [10] is solved using an iterative solver [11] in real space, which could be imple-

* Corresponding author.

E-mail address: rewoldt@pppl.gov (G. Rewoldt).

mented with good accuracy for arbitrary wavelengths of interest (modes with $k_\theta \rho_i \sim 1.5$ are resolved in simulations reported in this paper). A global field-aligned mesh in magnetic coordinates is constructed without any approximations in the geometry or the physics model.

Electron dynamics is implemented in the GTC code using an electrostatic version of a fluid-kinetic hybrid electron model [10] with an expansion of the electron response based on a smallness parameter of the ratio of the sound speed to the electron thermal speed, i.e. the square-root of electron-to-ion mass ratio. This hybrid model circumvents the electron Courant condition and removes the high frequency ω_H mode [10]. In the lowest order, electron response is adiabatic. Linear and nonlinear kinetic effects of electrons are retained in higher orders in the expansion. While the first order in the expansion accurately reproduces both linear and nonlinear Landau resonances in slab geometry, the second order in the expansion is needed to accurately describe the response of magnetically trapped particles in toroidal geometry [12]. In the linear simulations reported in this paper, the response of passing particles is mostly adiabatic.

GT3D solves the gyrokinetic Vlasov–Poisson system based on the Hamiltonian formalism [13]. In principle, kinetic electrons can be described by taking the drift-kinetic limit of the gyrokinetic equation. However, a full drift-kinetic model involves a high frequency mode (the kinetic Alfvén wave in the electrostatic limit) with $\omega_H = \sqrt{m_i/m_e}(k_\parallel/k_\perp)\Omega_i$ [14], and it is an expensive model for the TEM, which is a low frequency mode excited by toroidal precession of trapped electrons. To avoid the high frequency mode, we have implemented a drift-kinetic trapped electron model with adiabatic passing electron response. The limitation on the time step in the drift-kinetic trapped electron model, $\Delta t < \omega_{be}^{-1}$, is an order of magnitude longer than that in the full drift-kinetic model, $\Delta t < \omega_H^{-1}$, and the computational cost is significantly reduced, where ω_{be} is the trapped electron bounce frequency. From linear test calculations, we have confirmed that both models give almost the same real frequency and growth rate spectra for the ITG and TEM modes, indicating that passing electrons respond almost adiabatically to the TEM, at least in the linear regime. Therefore, in the present linear benchmark calculations, the drift-kinetic trapped electron model is used. Recently, the model has been improved based on a bounce-averaged kinetic equation [15], in which the fast electron bounce motion is averaged out under the bounce-kinetic ordering $\omega/\omega_{be} \ll 1$. In the bounce-averaged trapped electron model, the limitation on the time step is further relaxed to be comparable to that in the ITG turbulence simulation, and also the convergence is improved due to the absence of the ballistic noise coming from electron bounce motion. In Ref. [16], linear benchmark calculations showed good agreement for the ITG-TEM spectra obtained by the drift-kinetic and bounce-averaged trapped electron models.

Another extension of the code for TEM calculations is the treatment of the ion polarization density, $1 - I_0(b)e^{-b}$, in the gyrokinetic Poisson equation, where I_0 is the 0-th order modified Bessel function, $b = k_\perp^2 \rho_i^2$, and $\rho_i \equiv \sqrt{T_i/m_i}/(eB_0/m_i c)$. For the ITG modes with adiabatic electrons, which are un-

stable for $k_\theta \rho_i < 0.6$, a Taylor expansion model with $b \ll 1$, $1 - I_0(b)e^{-b} \sim b$, is a relatively good approximation. On the other hand, in analyzing the ITG-TEM modes, which have a broad unstable spectrum up to a short wavelength region with $k_\theta \rho_i \geq 0.6$, we use a Pade approximation model, $1 - I_0(b)e^{-b} \sim b/(1+b)$ [17]. In Refs. [16,18], these two models were implemented for a global gyrokinetic Poisson solver based on a finite element approximation, and the applicability of the model was discussed.

3. Case for comparison

All of the codes for the present comparison are in the collisionless, electrostatic limit, and employ a model toroidal geometry with circular, concentric magnetic surfaces. On a reference magnetic surface at radius $r = r_0 = 0.5a$, where a is the plasma boundary radius, all three codes use identical local parameters called the ‘‘Cyclone parameters’’, originally given in Ref. [19]. On this surface, in standard notation, they are: $r/R = 0.18$, $q = 1.4$, $\hat{s} = q'r/q = 0.776$, $T_e/T_i = 1.0$, $R/L_n = R/L_{ne} = R/L_{ni} = 2.22$, where $L_{nj} \equiv -(d \ln n_j/dr)^{-1}$, $R/L_{T_e} = R/L_{T_i} = 6.92$, where $L_{Tj} \equiv -(d \ln T_j/dr)^{-1}$ [so that $\eta_e = \eta_i = 3.114$, where $\eta_j \equiv (d \ln T_j/dr)/(d \ln n_j/dr)$], and $k_\theta \rho_i = 0.335$, where $k_\theta \equiv nq/r$, and n is the toroidal mode number. Starting from this initial set of parameters, we will vary $k_\theta \rho_i$ (evaluated at the reference surface), with adiabatic electrons and with trapped electrons, and also R/L_{T_i} (and thus η_i) (evaluated at the reference surface), with trapped electrons, and compare the linear eigenfrequency results for the ITG root and the TEM root. The units for the growth rates and real frequencies are c_s/L_n (evaluated at the reference surface), where $c_s \equiv \sqrt{T_e/m_i}$.

The three codes differ away from this reference magnetic surface. The FULL code is radially local; thus, it only knows about the density and temperature values and gradients on the reference surface with $r = r_0 = 0.5a$. The GT3D code uses the density profiles $n_e(r) = n_i(r) = n_0 \exp\{-(\Delta_r/L_n) \tanh[(r - r_0)/\Delta_r]\}$ and the temperature profiles $T_j(r) = T_{0j} \exp\{-(\Delta_r/L_{Tj}) \tanh[(r - r_0)/\Delta_r]\}$, with the density and temperature gradients being obtained from these expressions, and with $a/\rho_i \simeq 150$. The q -profile is given by $q(r) = q_0 + q_2(r/a)^2$, with $q_0 = 0.854$ and $q_2 = 2.184$. The GTC code uses the density gradient parameter profile $\kappa_n(r) \equiv -(Rd \ln n/dr) = \kappa_{n0} \exp\{-[(r - r_0)/\delta_r]^6\}$ and the temperature gradient parameter profile $\kappa_{Tj}(r) \equiv -(Rd \ln T_j/dr) = \kappa_{Tj0} \exp\{-[(r - r_0)/\delta_r]^6\}$ for the radially-varying density and temperature gradients, with the same $q(r)$ profile as for GT3D, and with $a/\rho_i \simeq 125$. However, the GTC code, unlike the GT3D code, takes the density and temperature values (but not the gradients) to be constant in radius, so that, in particular, the ion gyro-radius is constant in radius. Both codes use marker particle distributions given by a local Maxwellian distribution. It will be seen that the results from the GT3D and GTC are in acceptable agreement despite these differences in the input density and temperature profile shapes.

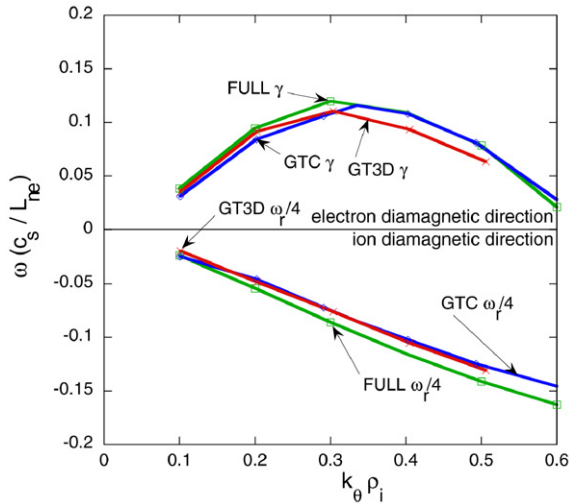


Fig. 1. Results for varying $k_{\theta} \rho_i \propto n$ at fixed $R/L_{Ti} = R/L_{Te} = 6.92$, $R/L_n = 2.22$ (on reference surface) with adiabatic electron response.

4. Results

For the parameters listed in Section 3, first in the adiabatic electron limit, for which only the ion temperature gradient (ITG) mode is obtained, $k_{\theta} \rho_i \propto n$ is varied. The results from the three codes are shown in Fig. 1. There is good agreement among the three codes. The ITG mode linear growth rate γ has a maximum around $k_{\theta} \rho_i = 0.3$ for this case. The real frequency ω_r increases monotonically with $k_{\theta} \rho_i$ and is in the ion diamagnetic direction (negative in this sign convention), as expected for the ITG mode.

The corresponding results for varying $k_{\theta} \rho_i$ including the effects of trapped electrons are shown in Fig. 2(a) for γ and in Fig. 2(b) for ω_r . When trapped electron effects are included for this case, there are two roots, one corresponding to the trapped-electron mode and one to the ion temperature gradient mode. The ITG root has the higher growth rate at smaller values of $k_{\theta} \rho_i$, and the TEM root has the higher growth rate at larger values of $k_{\theta} \rho_i$. The FULL code, as an eigenvalue code, can find any unstable root, even when the root in question is not the most unstable root. The GTC and GT3D codes, on the other hand, as initial-value codes always find the most unstable root. Thus, when the growth rate curves for the two roots cross, these two codes will jump from one root to the other, with a corresponding jump in the real frequency. For the FULL code, then, there are two curves over the entire range in $k_{\theta} \rho_i$, corresponding to the two roots, in each of these figures, with the growth rate curves crossing at about $k_{\theta} \rho_i = 0.6$. For the GTC and GT3D codes, on the other hand, there is a single composite growth rate curve for each code with a change in slope at about this $k_{\theta} \rho_i$ value, and two segments of the real frequency curve for each code, corresponding to the two roots. The ITG root has a real frequency in the ion diamagnetic direction and the TEM root has a real frequency in the electron diamagnetic direction (positive in this sign convention). The ITG growth rate curve again has a maximum for $k_{\theta} \rho_i \simeq 0.3$ for all three codes, whereas the TEM growth rate curve almost plateaus after an initial increase. The real frequency curves again monotonically increase in magni-

tude with $k_{\theta} \rho_i$. The agreement among the three codes for γ and ω_r is acceptable. Also, note that the maximum (over $k_{\theta} \rho_i$) growth rate for the ITG root almost doubles due to the addition of trapped electron effects to the previous adiabatic electron response.

A corresponding scan over $k_{\theta} \rho_i$ for $R/L_{Ti} = 2.22$ ($\eta_i = 1.0$), again for $R/L_{Te} = 6.92$ and $R/L_n = 2.22$, is shown in Fig. 3 (a) and (b) for γ and ω_r , respectively. For this case, only the TEM root is unstable since $\eta_i = 1.0$ is below the critical value of η_i for the ITG root to be unstable. Again, the agreement among the three codes is satisfactory.

The variations of γ and ω_r with R/L_{Ti} , at fixed $R/L_{Te} = 6.92$, $R/L_n = 2.22$, and $k_{\theta} \rho_i = 0.335$, are shown in Fig. 4 (a) and (b), respectively. Again, the FULL code can track the TEM root and the ITG root separately over their respective unstable ranges in R/L_{Ti} , and they are shown as separate curves in the figures. The GTC and GT3D codes again automatically find the most unstable root for a given value of R/L_{Ti} , and there is thus a change of slope in their growth rate curves and a jump in their real frequency curves where the growth rate curves for the two roots cross, near $R/L_{Ti} = 5.5$ ($\eta_i = 2.5$). Keeping this in mind, the agreement in the eigenfrequencies among the three codes is again acceptable.

The corresponding eigenfunctions for some of these cases are shown in Figs. 5, 6 and 7, for $R/L_n = 2.22$, $R/L_{Te} = 6.92$, and $k_{\theta} \rho_i = 0.335$. The eigenfunctions from the FULL code are plotted in Fig. 5 versus the non-periodic ballooning representation variable θ , which shows the variation along the equilibrium magnetic field lines. Both eigenfunctions are localized around $\theta = 0$, but the TEM root eigenfunction in Fig. 5(a), for $\eta_i = 1.00$ ($R/L_{Ti} = 6.66$) is somewhat more localized than that for the ITG root eigenfunction in Fig. 5(b), for $\eta_i = 3.00$ ($R/L_{Ti} = 6.66$). The GTC code eigenfunctions for the individual poloidal harmonics, versus r/a , are shown in Fig. 6(a) for the TEM root for $\eta_i = 1.00$ ($R/L_{Ti} = 2.22$), and in Fig. 6(b) for the ITG root for $\eta_i = 3.12$ ($R/L_{Ti} = 6.92$). The individual poloidal harmonics are centered on their respective mode-rational surfaces at r_{mn} , where $q(r_{mn}) = m/n$, with roughly comparable widths for each poloidal harmonic. However, the overall radial envelope for the ITG root at $\eta_i = 3.12$ is substantially broader than that for the TEM root at $\eta_i = 1.00$. The GT3D code eigenfunctions for the individual poloidal harmonics, versus r/a , are shown in Fig. 7(a) for the TEM root for $\eta_i = 1.00$ ($R/L_{Ti} = 2.22$), and in Fig. 7(b) for the ITG root for $\eta_i = 3.00$ ($R/L_{Ti} = 6.66$). Again, the individual poloidal harmonics are centered on their respective mode-rational surfaces at r_{mn} , with roughly comparable widths for each poloidal harmonic, which are also comparable to those for GTC. For GT3D, the overall radial envelope for the ITG root for $\eta_i = 3.00$ is slightly broader than that for the TEM root at $\eta_i = 1.00$. The radial envelopes for the GTC eigenfunctions are shifted outward somewhat relative to the GT3D envelopes, due to the differences in the density and temperature value and gradient profile shapes, as described previously. The actual values of the toroidal and poloidal harmonic numbers are also different between GTC and GT3D, due to the use of different reference temperature values, so as to have the same reference $k_{\theta} \rho_i$ values.

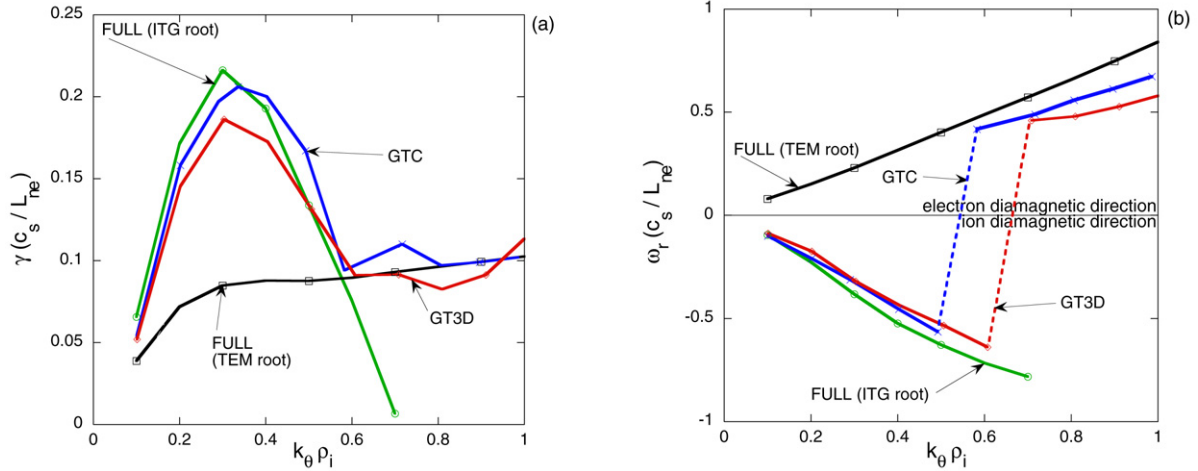


Fig. 2. Results for varying $k_{\theta} \rho_i \propto n$ at fixed $R/L_{T_i} = R/L_{T_e} = 6.92$, $R/L_n = 2.22$ (on reference surface), including trapped electron response.

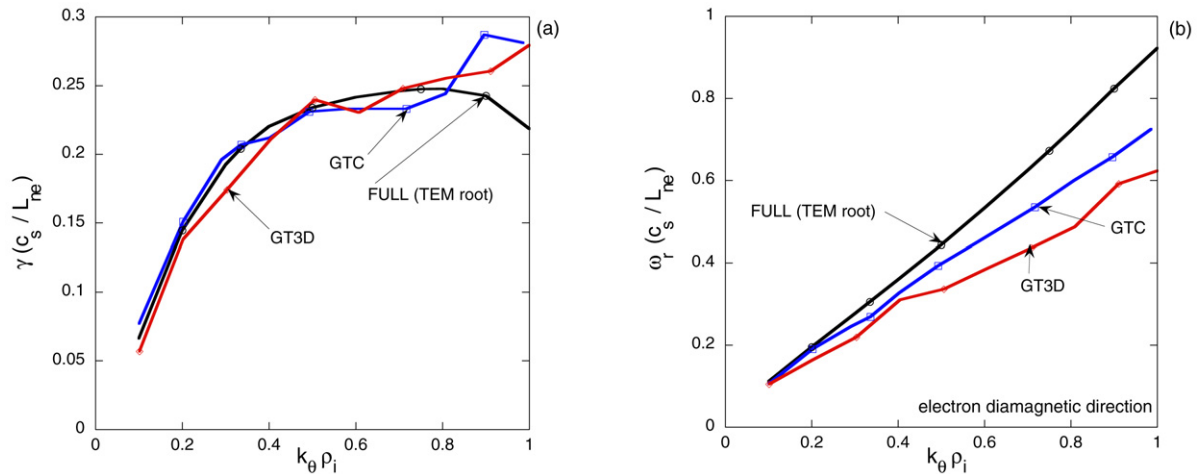


Fig. 3. Results for varying $k_{\theta} \rho_i \propto n$ at fixed $R/L_{T_i} = 2.22$, $R/L_{T_e} = 6.92$, $R/L_n = 2.22$ (on reference surface), including trapped electron response.

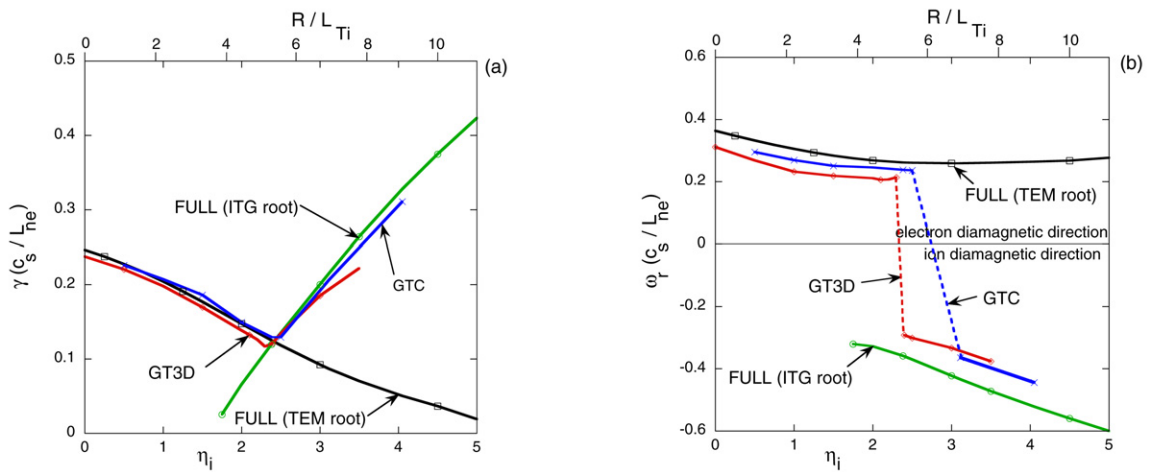


Fig. 4. Results for varying R/L_{T_i} at fixed $R/L_{T_e} = 6.92$, $R/L_n = 2.22$ and $k_{\theta} \rho_i = 0.335$ (on reference surface), including trapped electron response.

5. Conclusions

The GT3D and GTC codes now include trapped-electron effects, while the FULL code has included trapped-electron

effects since the beginning. Adding these effects introduces a new unstable root, the TEM root, in addition to increasing the growth rate of the previous root, the ITG root. For the present parameters, these two roots remain separate, while

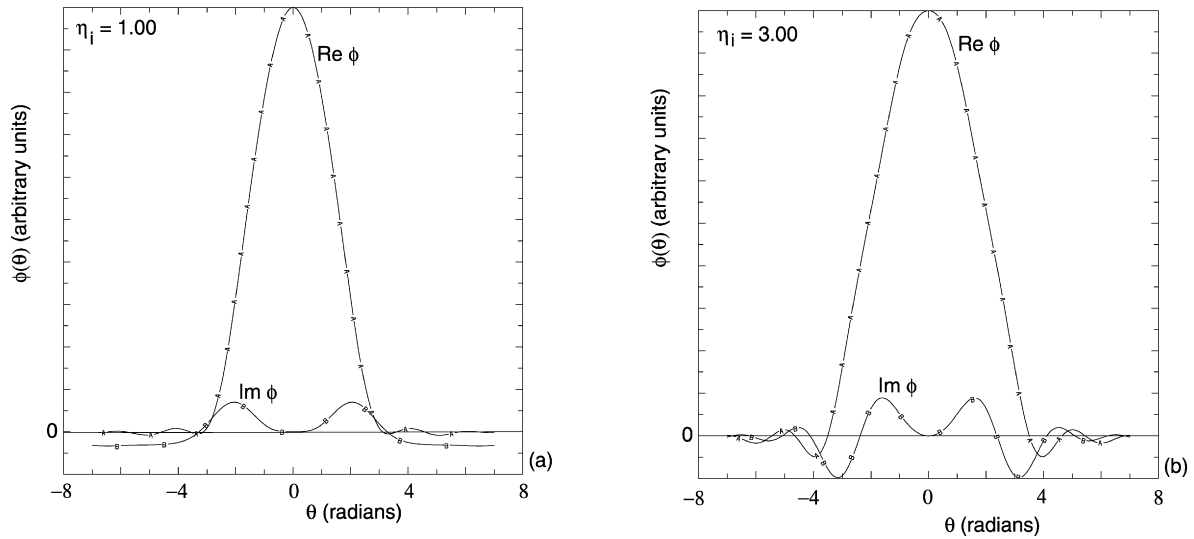


Fig. 5. Eigenfunctions from FULL code versus θ (nonperiodic variable along field line) for: (a) TEM root with $\eta_i = 1.00$ ($R/L_{Ti} = 2.22$) and (b) ITG root with $\eta_i = 3.00$ ($R/L_{Ti} = 6.66$).

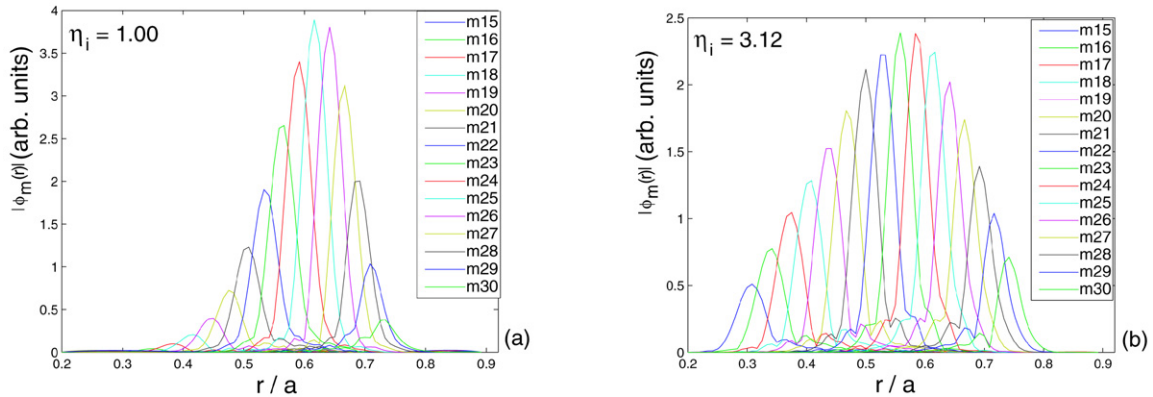


Fig. 6. Eigenfunctions from GTC code versus r/a for: (a) TEM root with $\eta_i = 1.00$ ($R/L_{Ti} = 2.22$) and (b) ITG root with $\eta_i = 3.12$ ($R/L_{Ti} = 6.92$) for individual poloidal harmonics.

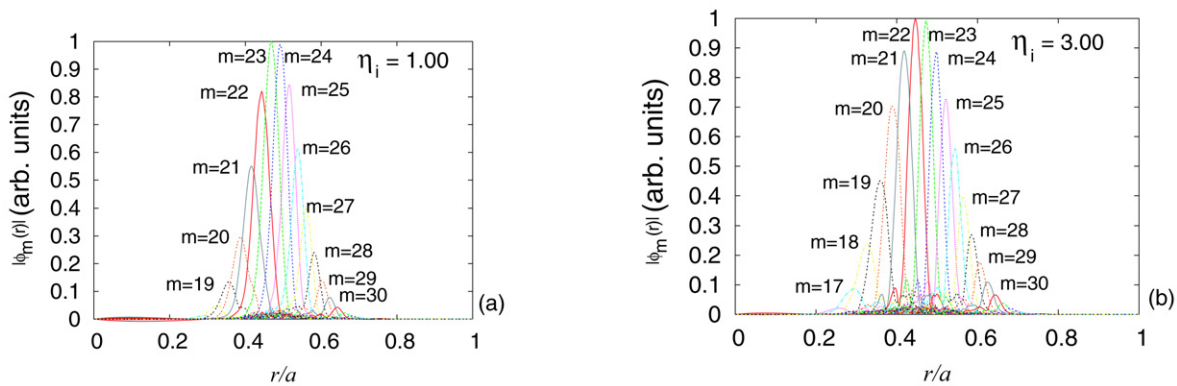


Fig. 7. Eigenfunctions from GT3D code versus r/a for: (a) TEM root with $\eta_i = 1.00$ ($R/L_{Ti} = 2.22$) and (b) ITG root with $\eta_i = 3.00$ ($R/L_{Ti} = 6.66$) for individual poloidal harmonics.

for other parameters the two roots can “hybridize” to form a single ITG-TEM root [20]. These trapped-electron destabilization effects arise mainly due to the resonant collisionless trapped-electron mode destabilization mechanism, due to resonances between the mode eigenfrequency and the

orbit-time-average magnetic drift frequency (precession frequency) [3].

Scans over R/L_{Ti} (η_i) and $k_{\theta} \rho_i$ show reasonably good agreement on the linear growth rates and real frequencies for both the ITG root and the TEM root among the GTC, GT3D,

and FULL codes. This is true despite some differences among the three codes in the radial variation (away from the reference surface) of the input density and temperature values and gradients.

The present comparison is only for linear growth rates and real frequencies and linear eigenfunctions. A task for the future is extending the comparison among nonlinear gyrokinetic codes to the nonlinear levels of particle and energy transport.

Acknowledgements

Figure 6 was provided by Dr. Yong Xiao. This work was supported by U.S. DOE Contract No. DE-AC02-76-3073 at PPPL and by U.S. DOE Cooperative Agreement No. DE-FC02-04ER54796 at U.C.-Irvine. One of the authors (Y.I.) was supported by the Japanese Ministry of Education, Culture, Sports, Science, and Technology, Grant No. 18760647.

References

- [1] Z. Lin, T.S. Hahm, W.W. Lee, W.M. Tang, R.B. White, *Science* 281 (1998) 1835.
- [2] Y. Idomura, S. Tokuda, Y. Kishimoto, *Nucl. Fusion* 43 (2003) 234.
- [3] G. Rewoldt, W.M. Tang, M.S. Chance, *Phys. Fluids* 25 (1982) 480.
- [4] G. Rewoldt, W.M. Tang, R.J. Hastie, *Phys. Fluids* 30 (1987) 807.
- [5] E.A. Frieman, G. Rewoldt, W.M. Tang, A.H. Glasser, *Phys. Fluids* 23 (1980) 1750.
- [6] M. Kotschenreuther, G. Rewoldt, W.M. Tang, *Comput. Phys. Comm.* 88 (1995) 128.
- [7] C. Bourdelle, W. Dorland, X. Garbet, G.W. Hammett, M. Kotschenreuther, G. Rewoldt, E.J. Synakowski, *Phys. Plasmas* 10 (2003) 2881.
- [8] E.A. Belli, W. Dorland, G.W. Hammett, M.C. Zarnstorff, *Bull. Am. Phys. Soc.* 46 (8) (2001) 232.
- [9] R.B. White, M.S. Chance, *Phys. Fluids* 27 (1984) 2455.
- [10] Z. Lin, L. Chen, *Phys. Plasmas* 8 (2001) 1447.
- [11] Z. Lin, W.W. Lee, *Phys. Rev. E* 52 (1995) 5646.
- [12] Y. Nishimura, Z. Lin, W.X. Wang, *Phys. Plasmas* 14 (2007) 042503.
- [13] T.S. Hahm, *Phys. Fluids* 31 (1988) 2670.
- [14] W.W. Lee, *J. Comput. Phys.* 72 (1987) 243.
- [15] B.H. Fong, T.S. Hahm, *Phys. Plasmas* 6 (1999) 188.
- [16] Y. Idomura, S. Tokuda, Y. Kishimoto, *J. Plasma Fusion Res.* 6 (2004) 17.
- [17] G. Hammett, W. Dorland, F.W. Perkins, *Phys. Fluids B* 4 (1992) 2052.
- [18] A. Bottino, T.M. Tran, O. Sauter, J. Vaclavik, L. Villard, in: J.W. Connor, O. Sauter, E. Sindoni (Eds.), *Theory of Fusion Plasmas: Proc. Joint Varenna-Lausanne International Workshop 2000*, Società Italiana di Fisica, Bologna, 2000, p. 327.
- [19] A.M. Dimits, G. Bateman, M.A. Beer, et al., *Phys. Plasmas* 7 (2000) 969.
- [20] G. Rewoldt, W.M. Tang, *Phys. Fluids B* 2 (1990) 318.